Neuron 49, 81–94, January 5, 2006 ©2006 Elsevier Inc. DOI 10.1016/j.neuron.2005.10.035

Two-Photon Imaging Reveals Somatodendritic Chloride Gradient in Retinal ON-Type Bipolar Cells Expressing the Biosensor Clomeleon

Jens Duebel,[1] Silke Haverkamp,[2] Wolfram Schleich,[3] Guoping Feng,[4] George J. Augustine,[4] Thomas Kuner,[3,*] and Thomas Euler[1,*]
[1] Department of Biomedical Optics
Max-Planck-Institute for Medical Research
Jahnstrasse 29
D-69120 Heidelberg
Germany
[2] Department of Neuroanatomy
Max-Planck-Institute for Brain Research
Deutschordenstrasse 46
D-60528 Frankfurt/Main
Germany
[3] Department of Cell Physiology
Max-Planck-Institute for Medical Research
Jahnstrasse 29
D-69120 Heidelberg
Germany
[4] Department of Neurobiology
Duke University Medical Center
Durham, North Carolina 27710

Summary

A somatodendritic gradient of Cl^- concentration ($[Cl^-]_i$) has been postulated to generate GABA-evoked responses of different polarity in retinal bipolar cells, hyperpolarizing in OFF cells with low dendritic $[Cl^-]_i$, and depolarizing in ON cells with high dendritic $[Cl^-]_i$. As glutamate released by the photoreceptors depolarizes OFF cells and hyperpolarizes ON cells, the bipolars' antagonistic receptive field (RF) could be computed by simply integrating glutamatergic inputs from the RF center and GABAergic inputs from horizontal cells in the RF surround. Using ratiometric two-photon imaging of Clomeleon, a Cl^- indicator transgenically expressed in ON bipolar cells, we found that dendritic $[Cl^-]_i$ exceeds somatic $[Cl^-]_i$ by up to 20 mM and that GABA application can lead to Cl^- efflux (depolarization) in these dendrites. Blockers of Cl^- transporters reduced the somatodendritic $[Cl^-]_i$ gradient. Hence, our results support the idea that ON bipolar cells employ a somatodendritic $[Cl^-]_i$ gradient to invert GABAergic horizontal cell input.

Introduction

In the outer retina, bipolar cells participate in computations that enhance contrast and prevent saturation. Two subclasses of bipolar cells respond with opposite signs to photoreceptor signals (Kaneko, 1970; Werblin and Dowling, 1969): ON bipolar cells are depolarized by light, whereas OFF bipolar cells are hyperpolarized. These responses are modulated by horizontal cells (Werblin, 1974; Werblin and Dowling, 1969), which are hyperpolarized by light (Kaneko, 1970). Horizontal cells monitor background light intensity and release more γ-aminobutyric acid (GABA) with decreasing illumination (reviewed in Schwartz, 2002). They can affect bipolar cell signaling via two pathways: indirectly by modulating the photoreceptor output, or directly via GABAergic input to the bipolars' dendrites (Hare and Owen, 1996; Toyoda and Kujiraoka, 1982; Werblin, 1974; Yang and Wu, 1991). As a result, bipolar cells exhibit receptive fields with antagonistic organization (Dacey et al., 2000; Hare and Owen, 1990; Stone and Schutte, 1991; Werblin and Dowling, 1969).

As both classes of bipolar cells possess dendritic ionotropic GABA receptors (Enz et al., 1996; Greferath et al., 1994; Vardi and Sterling, 1994), GABA needs to depolarize ON bipolars and hyperpolarize OFF bipolars to provide appropriate modulatory inputs (Figure 1). Hence, the same ion channel would have to mediate Cl^- efflux in ON bipolars but Cl^- influx in OFF bipolars. Depending on the relationship between chloride reversal potential (E_{Cl}) and resting potential (E_R), Cl^- currents can indeed mediate hyperpolarization as well as depolarization through the same ion channel. If $E_{Cl} > E_R$, the opening of Cl^- channels leads to Cl^- efflux and depolarization. Therefore, a high dendritic chloride concentration ($[Cl^-]_i$) in ON bipolars would give rise to depolarizing responses to GABA, while a low dendritic $[Cl^-]_i$ in OFF bipolars would produce hyperpolarizing responses (Miller and Dacheux, 1983; Vardi and Sterling, 1994).

Several lines of evidence support this hypothesis for the action of GABA in bipolar cells. The mechanisms creating the surround of bipolars are sensitive to a reduction in extracellular $[Cl^-]$ (Miller and Dacheux, 1976). Chloride activity measurements using ion-sensitive electrodes in mudpuppy retina suggest that the $[Cl^-]_i$ in ON bipolars is high enough to support Cl^- efflux ($E_{Cl} > E_R$) and, thus, GABA-mediated depolarization (Miller and Dacheux, 1983). To reconcile the observed high $[Cl^-]_i$ with their finding that GABA hyperpolarized ON bipolars, Miller and Dacheux (1983) proposed a $[Cl^-]_i$ gradient, with GABA causing hyperpolarization through receptors located at the axon terminals, where $[Cl^-]_i$ would be low. High dendritic $[Cl^-]_i$ in ON bipolar cells is also consistent with the specific expression of the Cl^--accumulating transporter NKCC1 (Na^+-K^+-$2Cl^-$ cotransporter) in their dendrites (Vardi et al., 2000). Conversely, OFF bipolar cells express KCC2 (K^+-$2Cl^-$ cotransporter), a Cl^- extruder, and therefore maintain low $[Cl^-]_i$. Using perforated patch-clamp recordings, three studies have determined dendritic GABA responses in subclasses of bipolar cells: Billups and Attwell (2002) found a small $[Cl^-]_i$ gradient in ON bipolar cells; however, they concluded that this gradient was too small to cause GABA to depolarize the dendrites of these cells. Focal GABA application to the outer plexiform layer (OPL) elicited depolarizing responses only in rod bipolar cells (Satoh et al., 2001), which have recently shown to possess a significant axodendritic $[Cl^-]_i$ gradient (Varela et al., 2005). Nonetheless, estimating $[Cl^-]_i$ by electrically measuring E_{Cl} immanently bears the risk of

*Correspondence: teuler@mpimf-heidelberg.mpg.de (T.E.); thomas.kuner@mpimf-heidelberg.mpg.de (T.K.)

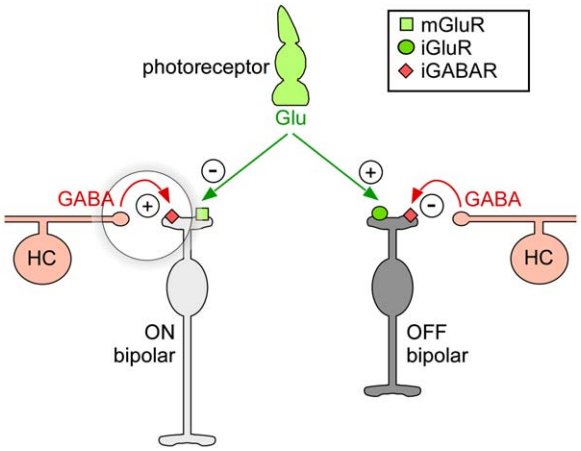

Figure 1. Modulation of Bipolar Cell Signals in the Outer Retina

Glutamate (Glu) released from photoreceptors hyperpolarizes (indicated by "−") ON bipolar cells via metabotropic Glu receptors (mGluR) but depolarizes ("+") OFF bipolar cells via ionotropic Glu receptors (iGluR). Bipolar cells are modulated by GABAergic input from horizontal cells (HC) via ionotropic GABA receptors (iGABAR). For further details, see Introduction.

perturbing the intracellular ionic composition—even when using Gramicidin perforated-patch recording (Akaike, 1994). Moreover, focal drug application is technically challenging, practically excluding spatially resolved measurements of $[Cl^-]_i$ in intact tissue.

To circumvent these problems, we applied two-photon (2p) imaging in combination with Clomeleon, a genetically encoded ratiometric Cl^- indicator (Kuner and Augustine, 2000), to directly image the spatiotemporal distribution of Cl^- in bipolar cells. For this purpose, we used transgenic mice expressing Clomeleon in a subset of retinal neurons including bipolar cells. We found a somatodendritic $[Cl^-]_i$ gradient enabling GABA-mediated Cl^- efflux (depolarization) in at least one subclass of ON bipolar cells.

Results

Clomeleon Expression in Transgenic Mice

Transgenic mouse lines expressing Clomeleon (CLM) were screened for expression of the Cl^- indicator in retinal bipolar cells. One of the lines, CLM1 (Figure 2A), showed robust expression of Clomeleon in a subset of bipolar cells, but also in ganglion cells (asterisk in Figure 2A) and amacrine cells (arrowhead in Figure 2A). The identification of morphological subtypes of labeled bipolar cells was hampered by the fact that processes of amacrine and ganglion cells expressing Clomeleon obscured the stratification pattern of the bipolar's axon terminals. Injection of fluorescent dye into single Clomeleon-positive bipolars circumvented this problem and revealed that these cells had their axon terminals in the inner half of the inner plexiform layer (IPL) (Figure 2B), suggesting that they are ON bipolar cells (reviewed in Ghosh et al., 2004). The morphology of these cells further allowed them to be identified as type 7, 8, and 9 cone bipolar cells (Ghosh et al., 2004).

A fourth type of bipolar cell, resembling type 2 (Ghosh et al., 2004), was occasionally found when Clomeleon-positive cells were visualized with an antibody against green fluorescent protein (GFP) (Figure 2C). It is unlikely, though, that this type of OFF bipolar was among the cells in our Cl^- imaging sample: First, all dye-injected Clomeleon-positive bipolar cells (n = 16) stratified in the inner half of the IPL, unlike type 2 cells. Second, in whole-mounted retina we usually traced the axon of the imaged Clomeleon-positive bipolars into the IPL and could follow it at least to the middle of the IPL. Finally, type 2 bipolars had a very low level of Clomeleon expression and therefore remained undetected in our Cl^- imaging experiments.

Figures 2D and 2E illustrate the differences in dendritic arbor shape and size between the Clomeleon-positive bipolar types in whole-mounted retina. Fixed tissue was intensified with anti-GFP antibody (green) and counterstained with an antibody against the glutamate receptor subunit 5 (GluR5; red) (Haverkamp et al., 2005) to visualize the cone pedicles. Type 9 cells (Figure 2D, asterisks) had sparse, long meandering dendrites, which particularly contact blue cone pedicles (examples encircled in Figure 2D). Type 8 cells (Figure 2E, open triangles) had thin, spiny dendrites and contact most cone pedicles in reach. The narrowly branching bipolar cells (filled triangles) with their short dendrites also seemed to contact all cone pedicles in reach. These were likely to be type 7 cells, but since this retina was GFP intensified, type 2 cells may be among those as well. In the living retina, we found this compact dendritic morphology only associated with type 7 bipolar cells. Unfortunately, none of the CLM mouse lines contained OFF bipolar cells with sufficiently high Clomeleon fluorescence to be studied.

In summary, our data indicate that virtually all of the intensely fluorescent bipolars in the retina of line CLM1 belong to the types 7, 8, and 9, offering an approach to study the intracellular Cl^- distribution in a defined subset of ON bipolar cells.

Calibration of $[Cl^-]_i$ Measurements

To calibrate the imaging setup for 2p excitation of Clomeleon, cultured neurons expressing Clomeleon were dialyzed with defined Cl^- concentrations via the patch pipette. Figure 3A shows fluorescence images of two such neurons before and after breaking in. In this example, the electrode contained 125 mM F^- to saturate the Clomeleon (Kuner and Augustine, 2000). After break-in, the yellow fluorescent protein (YFP) fluorescence of the cell (arrowhead) strongly decreased, due to quenching of the fluorophore by F^-. At the same time, cyan fluorescent protein (CFP) fluorescence increased due to a reduction in fluorescence resonance energy transfer (FRET) to the acceptor YFP. Equilibration of the cell with the pipette solution occurred within a few minutes (Figure 3B). Data points obtained with different $[Cl^-]$ in the pipette were well described by Equation 3 of the Experimental Procedures (Figure 3C). The calibration was used to convert raw two-channel YFP/CFP fluorescence images into pseudocolored $[Cl^-]_i$ maps (Figures 4, 5, and 7) that allowed visualization of local differences in $[Cl^-]_i$.

Steady-State $[Cl^-]_i$ in Different Bipolar Cell Compartments

To examine whether $[Cl^-]_i$ gradients exist in bipolar cells, we determined the steady-state $[Cl^-]_i$ in different

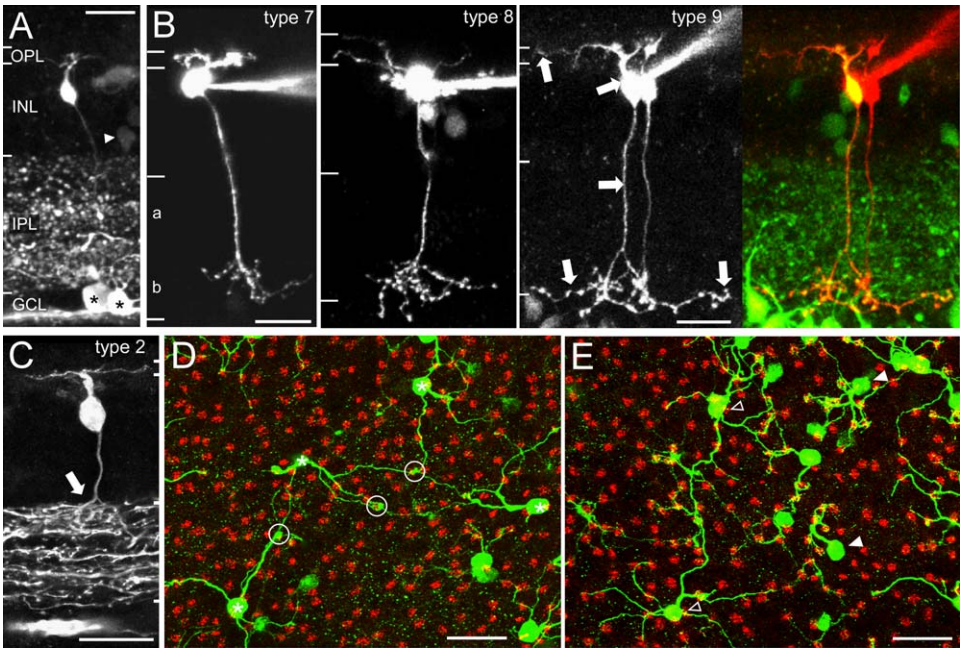

Figure 2. Clomeleon Expression in Transgenic Mouse Retina

(A) YFP fluorescence imaged with a two-photon microscope in a retinal slice expressing Clomeleon (collapsed image stack; OPL, outer plexiform layer; INL, inner nuclear layer; IPL, inner plexiform layer; GCL, ganglion cell layer). (B) Clomeleon-expressing bipolar cells injected with dye (classification according to Ghosh et al., 2004). Type 9 bipolar (rightmost panel; arrows) shown as overlay (green, Clomeleon; red, dye-injected; yellow, both) with coinjected Clomeleon-negative bipolar cell. (C) Anti-GFP antibody labeling of a weakly Clomeleon-expressing cell (fixed section) reveals cone bipolar resembling type 2 (arrowhead, axon stratifying in outer IPL). (D and E) Fixed whole-mounted retina colabeled with antibodies against GFP (green) and Glu receptor subunit 5 (red) revealing cone pedicles (collapsed image stacks; OPL to upper INL). Type 9 ([D]; asterisks) and type 8 ([E]; open arrowheads) cells can be distinguished from a third group of cells with compact dendritic trees ([E]; filled arrowheads), consisting of type 7 and possibly type 2 cells. Scale bars, 20 μm.

compartments of Clomeleon-positive bipolars in whole-mounted retinae. Image series of single cells were taken at different focal planes (Figure 4A): in the OPL (dendritic arbor), at the level of the soma, and just above the IPL (axon profile). Images of the axon terminals were not recorded, because we could not resolve the terminals among the other Clomeleon-containing processes in the IPL. Figures 4B–4D show three examples of such image sets. For each compartment, $[Cl^-]_i$ was determined by averaging pixels within regions of interest (ROIs) placed around the structures visible in the $[Cl^-]_i$ map.

The distribution of $[Cl^-]_i$ in the labeled population of bipolar cells is shown in Figure 4E (five retinae from five mice; 2–6 months old). ROIs in the OPL were placed such that they covered as much of the visible dendritic arbor as possible, including proximal dendrites. The average $[Cl^-]_i$ in dendrite, soma, and axon profile was 35 mM (±1; n = 104), 27 mM (±1; n = 118), and 25 mM (±2; n = 43), respectively. The variation in somatic $[Cl^-]_i$ between cells was relatively large: the somatic $[Cl^-]_i$ ranged from about 10 to 53 mM. However, in 90% of the cells ($range_{90\%}$) somatic $[Cl^-]_i$ was within the range of 15 to 36 mM (dendrites: 20 to 51 mM). To visualize the differences between $[Cl^-]_i$ in the three compartments, we plotted the dendritic and the axonal $[Cl^-]_i$ as a function of somatic $[Cl^-]_i$ (Figure 4E). The great majority of the dendritic data points were located above the unity line (dashed), indicating that $[Cl^-]_i$ was consistently higher in the dendrites than in the soma. The average difference between dendrite and soma (averaged over dendrite-soma pairs) of 9 ± 1 mM is statistically significant (n = 104 pairs; for statistic procedures used see Experimental Procedures). Most axonal data points were located on or below the unity line, thus the $[Cl^-]_i$ in the proximal axon tended to be slightly lower than in the soma (axon-soma: −2 ± 1 mM; n = 43 pairs), but this difference was not statistically significant.

The direction of Cl^- fluxes across the membrane depends on the difference between E_{Cl} and E_R. We used the Nernst equation to convert compartmental $[Cl^-]_i$ into "local" E_{Cl} (Figure 4F) and compared this with the known range of E_R for ON bipolar cells (−42 ± 10 mV, compiled from Euler and Masland, 2000; Euler and Wässle, 1998). For most cells, dendritic E_{Cl} was above the average E_R, indicating that E_{Cl} was less negative than E_R ($E_{Cl} > E_R$) in these dendrites. In these cases, opening of dendritic Cl^- channels should lead to Cl^- efflux and depolarization, so that GABAergic input to these dendrites could mediate excitation. A few cells had a dendritic E_{Cl} more negative than the average E_R ($E_{Cl} < E_R$), indicating that GABAergic input could cause Cl^- influx and inhibition of these dendrites. Since the net Cl^- flux scales with the absolute difference between E_{Cl} and E_R, these results indicated that the direct effect of GABAergic input on the membrane potential will greatly vary between bipolar cells. In cells were E_{Cl} was close to E_R, the net Cl^- flux may be so small that shunting inhibition is the predominant effect of GABA.

In theory, ratiometric measurements do not depend on fluorescence intensity (Grynkiewicz et al., 1985).

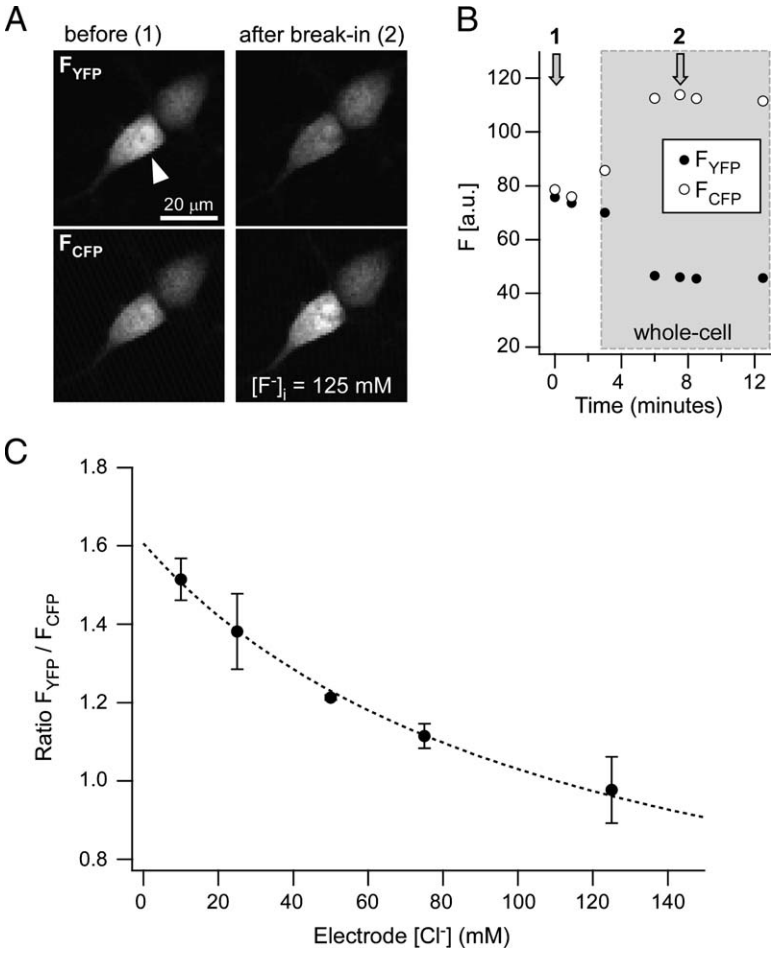

Figure 3. Calibration of $[Cl^-]_i$

(A) Cultured hippocampal neurons expressing Clomeleon before and after dialyzing one of the cells (arrowhead) with 125 mM F^- via a patch pipette. High $[F^-]$ mimics saturating $[Cl^-]$. (B) Fluorescence intensity for YFP and CFP as a function of time. Two arrows mark time points shown as images in (A) (gray area: whole-cell configuration). (C) Ratio of YFP/CFP fluorescence as a function of $[Cl^-]$ in the patch pipette and fitted calibration curve. Each data point represents a mean (± SEM) of three to six individual cells (n = 24 in total). Scale bar, 20 μm.

Nonetheless, we asked whether the lower intensity of Clomeleon fluorescence in the small structures of dendrites and axons biased our $[Cl^-]_i$ measurements. This was determined by examining the relationship between YFP intensity (F_{YFP}) and $[Cl^-]_i$ (Figure 4G). Although dendrites and axons had similar values for F_{YFP}, $[Cl^-]_i$ values measured in the two similarly small structures were quite different (mean difference: 11 ± 1 mM; n = 40; statistically significant). This indicates that the observed $[Cl^-]_i$ gradients are not due to differences in fluorescence intensity but instead reflect genuine differences in $[Cl^-]_i$.

$[Cl^-]_i$ Gradients Vary between Bipolar Cell Types

In the measurements described above, all Clomeleon-positive bipolar cells were pooled. To consider possible differences in $[Cl^-]_i$ gradient between bipolar types, we collected a second set of samples consisting only of cells that could be morphologically identified (six retinae from three mice; 2–5 months old). The dendritic $[Cl^-]_i$ was determined in ROIs positioned as distal as possible in the dendrites. Type 7 cells were identified by their dendritic tree size (Figure 2E). Their spiny distal dendritic tips were often weakly labeled, so that mostly the distal end of their primary dendrite was covered by the ROI (Figures 5A and 6B, right drawing). Type 9 cells were identified by the distinctive varicosities at their dendritic tips (Figures 2D and 5C). The ROI could be placed around the varicosities, because of their relatively strong fluorescence (Figures 5B and 5C and Figure 6B, left drawing). Type 8 cells possessed very thin dendrites with low fluorescence levels (Figures 2B and 2E), precluding reliable determinations of $[Cl^-]_i$. Therefore, we focused our efforts on type 7 and type 9 cells.

The mean somatic $[Cl^-]_i$ in type 7 cells was 21 ± 2 mM (n = 28; $range_{90\%}$: 9 to 30 mM; Figure 5A). In type 9 cells, we found a $[Cl^-]_i$ of 24 mM ± 2 (n = 40; $range_{90\%}$: 12 to 38 mM; Figures 5B and 5C). The somatic $[Cl^-]_i$ did not differ significantly between type 7 and type 9 cells, and both values were close to the mean somatic $[Cl^-]_i$ determined in the first sample of unselected cells. When plotting dendritic $[Cl^-]_i$ as a function of somatic $[Cl^-]_i$ (Figure 5D), the data points for type 7 lie close to the unity line, suggesting a small somatodendritic gradient. The data points for type 9 were shifted well above the line, indicating larger somatodendritic $[Cl^-]_i$ gradients. The distribution of somatodendritic $[Cl^-]_i$ gradients was different for each cell type (Figure 5E), with type 7 cells showing a more narrow range of $[Cl^-]_i$ than type 9 cells. The average somatodendritic difference was 4 ± 1 mM (n = 28 pairs) in type 7 cells and 20 ± 2 mM (n = 40 pairs) in type 9 cells. For both type 7 and type 9 cells, this difference between somatic and dendritic $[Cl^-]_i$ was statistically significant, suggesting that $[Cl^-]_i$ gradients exist in both cell types, although much more pronounced in type 9 cells.

The mean dendritic $[Cl^-]_i$ of type 7 cells was 25 ± 2 mM (n = 28; $range_{90\%}$: 14 to 39 mM); in type 9 it was 44 ± 3 mM (n = 40; $range_{90\%}$: 20 to 71 mM), yielding a statistically significant difference of 20 ± 3 mM. This difference

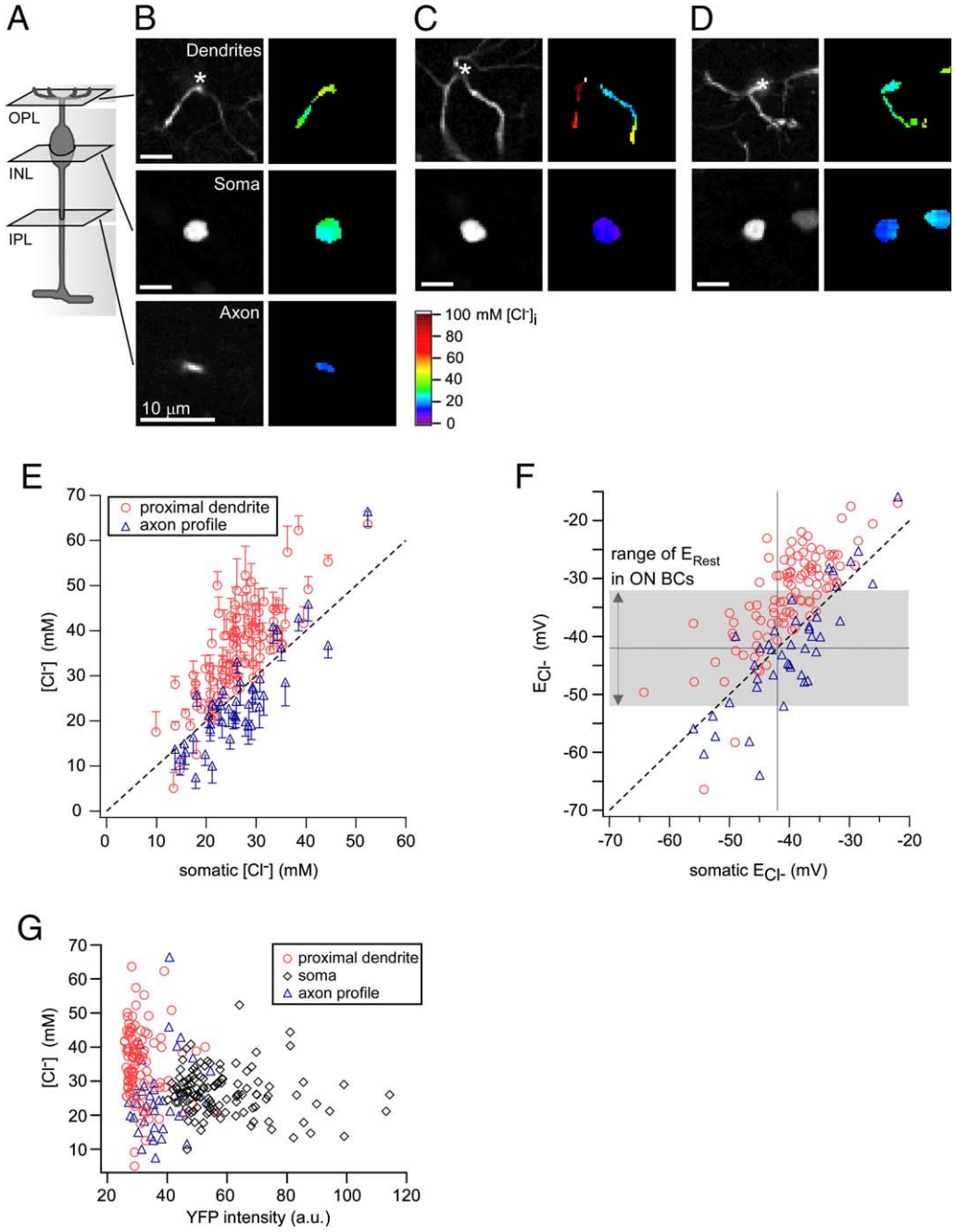

Figure 4. Steady-State $[Cl^-]_i$ in Different Compartments of Clomeleon-Positive Bipolar Cells in Whole-Mounted Retina

(A) Illustration of the three focal planes from which images were acquired. (B) Single focal planes of dendritic arbor, soma, and axon (above the IPL) for an unidentified, brightly fluorescent Clomeleon-positive bipolar cell (left panels, F_{YFP} illustrating morphology; right panels, corresponding color-coded $[Cl^-]_i$ maps; see Experimental Procedures). Asterisks denote soma position. $[Cl^-]_i$ maps only contain regions of fluorescence sufficiently strong for reliable measurements (see Experimental Procedures). (C and D) As in (B), but other examples. (E) Dendritic and axonal $[Cl^-]_i$ of Clomeleon-positive bipolars as a function of somatic $[Cl^-]_i$ (n = 104 cells; 43 of those with axonal $[Cl^-]_i$; data pooled from five animals; SEM shown as single-sided error bars represents variability between consecutive measurements). (F) Data from (E) but with $[Cl^-]_i$ converted into E_{Cl} (in mV; with T = 22°C; $[Cl^-]_o$ = 124 mM). Horizontal bar (gray) indicates known range of E_R (−42 ± 10 mV) for ON bipolar cells (see text). (G) $[Cl^-]_i$ for the different compartments (data from [E]) as a function of absolute YFP fluorescence intensity. Scale bars, 10 μm.

between type 7 and 9 cell dendrites may arise from the location of the ROIs, with $[Cl^-]_i$ measured at a more distal location in type 9 cells than in type 7 cells. Determinations of Cl^- reversal potentials indicate that the dendritic E_{Cl} of many type 9 cells was well above the mean E_R (Figure 5F), so that GABA would cause Cl^- efflux and depolarization of these dendrites. The dendritic E_{Cl} in type 7 cells is closer to E_R, suggesting that, at least in the more proximal parts of the dendrite imaged here, GABA-induced net Cl^- flux is smaller.

Our data demonstrate that at least one subset of bipolar cells exhibits a robust somatodendritic $[Cl^-]$ gradient

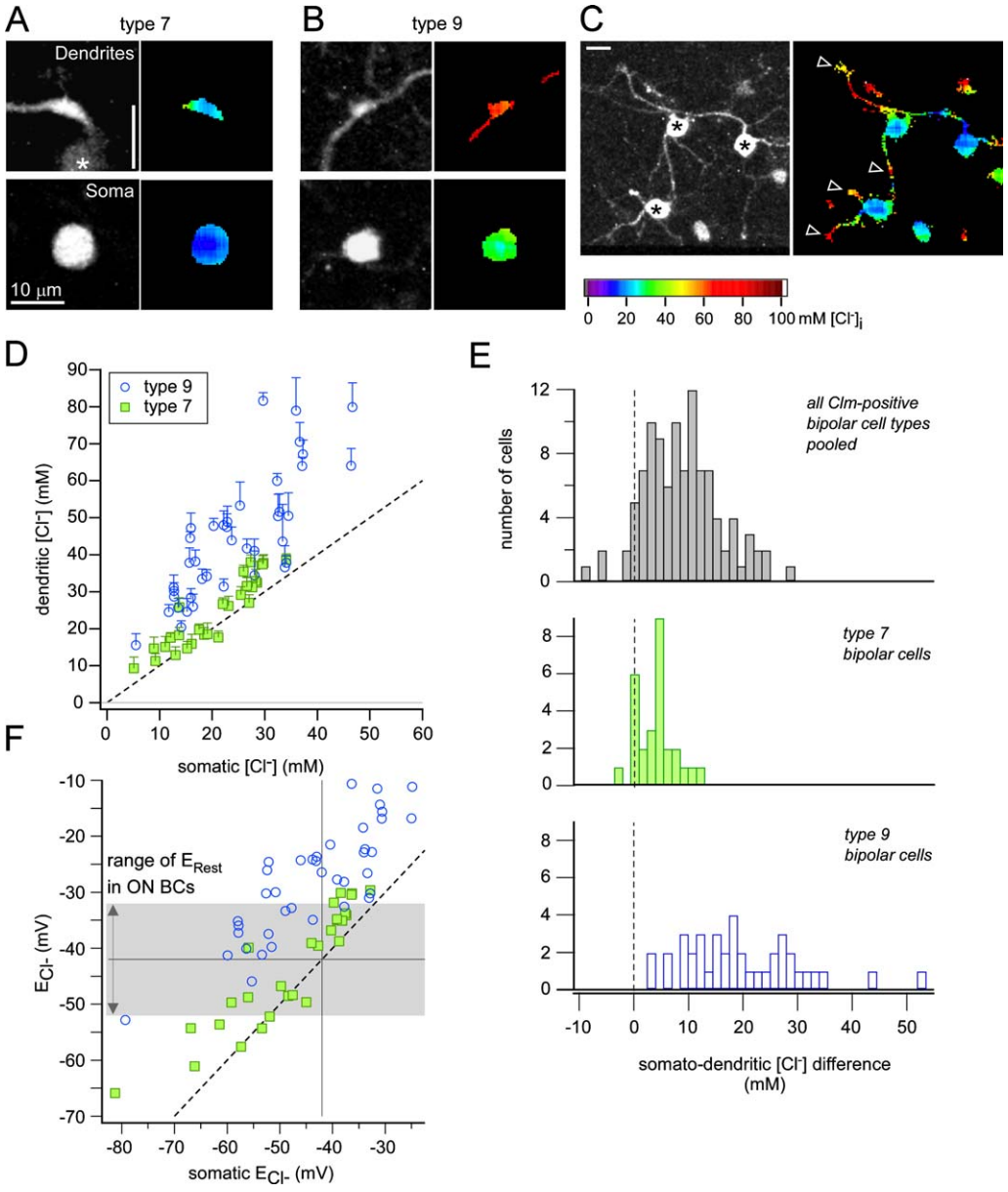

Figure 5. $[Cl^-]_i$ in Different Types of Clomeleon-Expressing Bipolar Cells in Whole-Mounted Retina

(A and B) Examples for a type 7 (A) and a type 9 (B) cell (single focal planes; left panels, morphology; right panels, color-coded $[Cl^-]_i$ maps). Soma position indicated in (A) (asterisk); outside the field of view in (B). (C) Group of type 9 bipolar cells (asterisks; collapsed image stack). $[Cl^-]_i$ high in varicosities (arrowheads). (D) Dendritic $[Cl^-]_i$ of Clomeleon-positive type 7 (green squares; n = 28) and type 9 (blue circles; n = 40) cells as a function of somatic $[Cl^-]_i$ (data pooled from three animals; SEM shown as single-sided error bars represents variability between consecutive measurements). (E) Histograms of Cl^- gradients (dendrite versus soma) for the sample of cells from Figure 4 (upper row), type 7 (middle row), and type 9 (bottom row). (F) Data from (D) but with $[Cl^-]_i$ converted into E_{Cl}. Horizontal bar (gray) indicates known range of E_R (−42 ± 10 mV) for ON bipolar cells. Scale bars, 10 μm.

with significantly higher $[Cl^-]_i$ in the dendrites (summarized in Figure 6). Where we also determined $[Cl^-]_i$ in axon profiles (Figure 6), we found a tendency toward lower $[Cl^-]_i$ in the axon, consistent with the observations that these axons receive hyperpolarizing GABAergic and glycinergic input (e.g., Suzuki et al., 1990).

To test if the Cl^- transporters NKCC and KCC (Vardi et al., 2000) are involved in generating the Cl^- gradient, we examined the actions of transporter inhibitors. We used furosemide (Fu), a rather nonselective NKCC/KCC blocker, and bumetanide (Bm), which is ~500-fold more effective on NKCC (reviewed in Payne et al., 2003). The actions of these inhibitors on $[Cl^-]_i$ gradients were measured in type 9 cells (n = 15; pooled from three animals; data not shown). In these experiments, GABA- and glycine-mediated synaptic transmission was blocked by picrotoxin (50 μM) and strychnine (1 μM) to prevent possible effects of the transport inhibitors on synaptic networks within the retina. Both the $[Cl^-]_i$ gradient (19 ± 2 mM) and absolute $[Cl^-]_i$ (soma: 24 ± 1 mM; dendrite: 43 ± 2 mM) of type 9 cells were indistinguishable from values measured in the absence of picrotoxin and

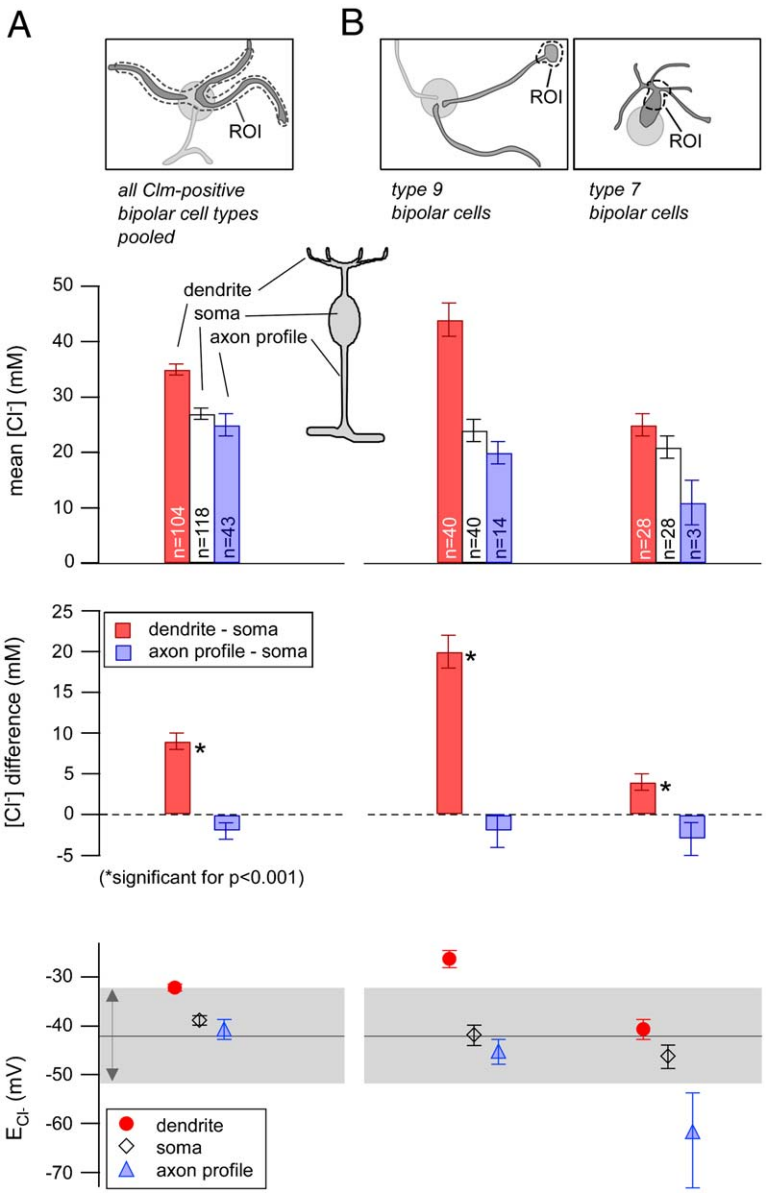

Figure 6. Summary of Steady-State $[Cl^-]_i$ Data

(A) Average $[Cl^-]_i$ by compartment, respective $[Cl^-]_i$ gradients, and resulting Cl^- reversal potentials for data set from Figure 4 (mean ± SEM; bottom row: gray horizontal bar indicates known range of E_R for ON bipolar cells). Schematic drawing (top) illustrating position and extent of a region of interest (ROI) for the dendritic measurement in the focal plane containing the dendritic arbor. Soma and out-of-focus dendrites are hinted in lighter gray.

(B) Different data set consisting of type 9 (left column) and type 7 (right column) bipolars.

strychnine, indicating that such networks do not significantly affect steady-state $[Cl^-]_i$ in the absence of Fu/Bm. We coapplied the transport inhibitors to maximize the effect on the $[Cl^-]_i$ gradient. Application of Fu/Bu (both 25 μM) for at least 30 min reduced the $[Cl^-]_i$ gradient to 14 ± 2 mM (soma: 22 ± 1 mM; dendrite: 36 ± 2 mM), corresponding to 68% ± 8% of the control value (statistically significant). Washing out the transport inhibitors restored the $[Cl^-]_i$ gradient to 18 ± 2 mM (soma: 20 ± 1 mM; dendrite: 38 ± 2 mM), corresponding to 101% ± 10% of the control value. Hence, NKCC and KCC contribute to the formation of the $[Cl^-]_i$ gradient, although this gradient also appears to require additional transport systems.

GABA-Evoked $[Cl^-]_i$ Changes

To evaluate the effect of high dendritic $[Cl^-]_i$ on bipolar cell function, we examined the GABA responses of bipolar cells. For this purpose, GABA (50–250 μM) was applied via a puffer pipette, and $[Cl^-]_i$ was measured in Clomeleon-positive bipolars in slices. No efforts were made to locally restrict application of GABA because the imaging approach allowed us to directly measure $[Cl^-]_i$ changes in a spatially resolved manner. To map responses in more than one focal plane, we sacrificed temporal resolution and recorded the $[Cl^-]_i$ distribution at multiple time points by capturing image stacks at several focal planes before, during, and after GABA application.

We found three types of GABA-evoked changes in $[Cl^-]_i$. The first type is illustrated in Figure 7A, which shows a (putative) type 7 cell. In this case, GABA induced a rise in $[Cl^-]_i$ that was restricted to the dendrite. Such responses were observed in 14 cells out of a total of 119 (12%). In a second group of cells, GABA application caused an efflux of $[Cl^-]_i$, either from both dendrites and somata (Figure 7B, upper row; unidentified bipolar) or just from the dendrites (Figure 7B, lower row; putative

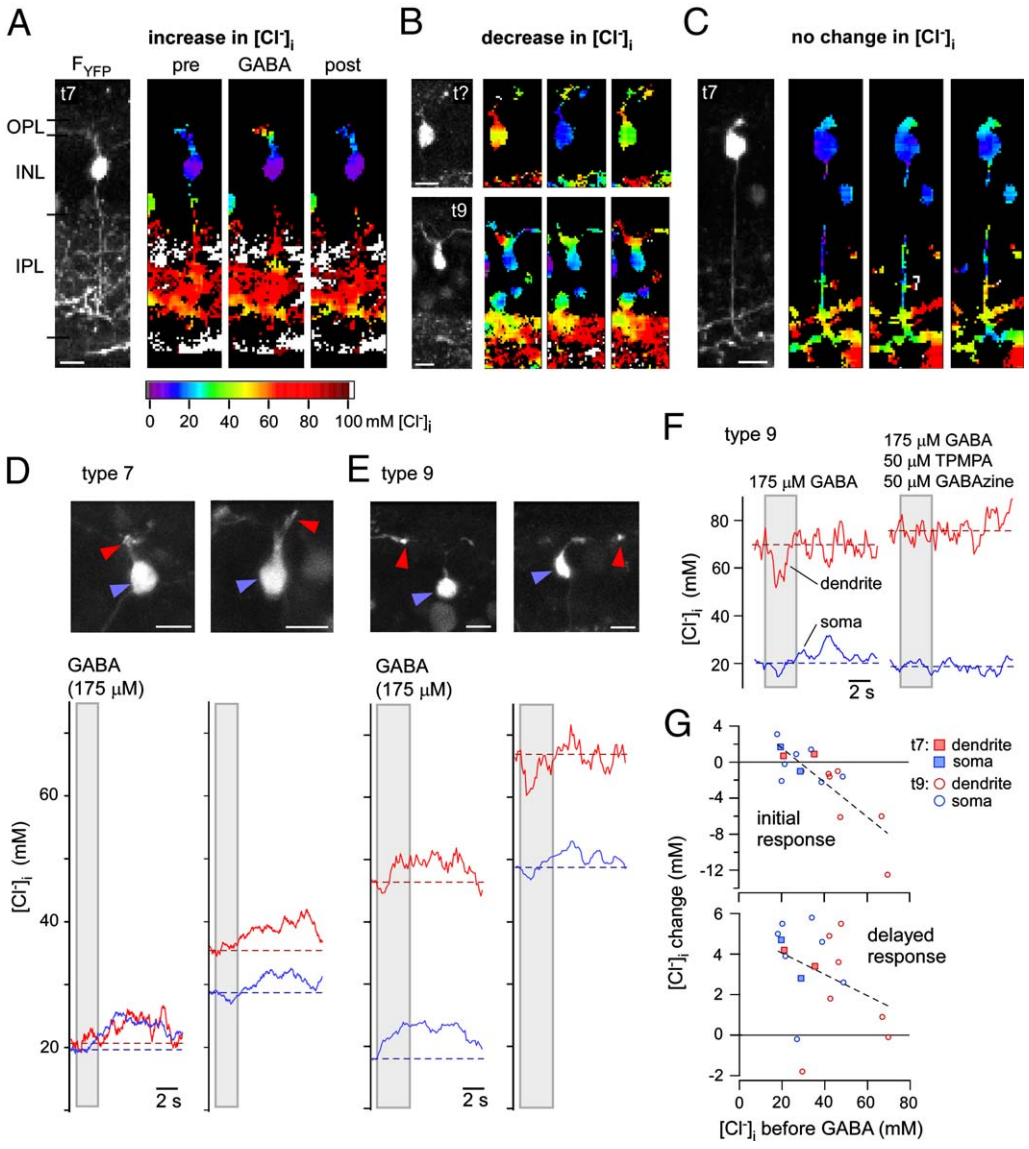

Figure 7. Effect of GABA Application on $[Cl^-]_i$ in Clomeleon-Positive Bipolar Cells in Retinal Slices

(A) Clomeleon-positive bipolar cell (putative type 7) imaged before, during, and after GABA application to the outer half of the slice using a puffer pipette. The high $[Cl^-]_i$ in the inner plexiform layer (IPL) reflects damage due to slicing. (B) GABA responses in an unidentified bipolar and in a putative type 9 cell. (C) Bipolar cells lacking detectable GABA-induced changes in $[Cl^-]_i$ (putative type 7). (D and E) Traces showing dendritic (red) and somatic (blue) $[Cl^-]_i$ in two type 7 and two type 9 bipolar cells during GABA application. Pictures illustrate position (arrowheads) of respective ROIs. Traces are averages of n = 5 (D) or 7 (E) trials. (F) Coapplication of GABA receptor antagonists TPMPA and GABAzine (average of n = 3 trials). (G) GABA-evoked $[Cl^-]_i$ change in dendrite (red) and soma (blue) as a function of resting $[Cl^-]_i$ for type 7 (squares) and type 9 cells (circles) (n = 9 cells). "Initial" response represents the mean determined in 0.5 s window placed within t = 0.5 to 2 s after start of application (top; Pearson's $\rho = -0.82$); "delayed" response indicates the mean of a 2 s window beginning at t = 4 s after application start (bottom; $\rho = -0.36$). Scale bars, 10 μm.

type 9). These responses were observed in 18 cells (15%). In the third group of cells, no GABA-evoked changes in $[Cl^-]_i$ were detected (Figure 7C). This was the case for 73% of the cells (87 out of 119 cells). For all cells that responded to GABA with a change in $[Cl^-]_i$, the direction of the Cl^- flux was consistent with the resting $[Cl^-]_i$: influx of Cl^- occurred in compartments with low resting $[Cl^-]_i$ (Figure 7A), while Cl^- efflux occurred in compartments with high resting $[Cl^-]_i$ (Figure 7B). Therefore, GABA applications produced a consistent pattern of changes in $[Cl^-]_i$. Furthermore, prolonged application of high GABA concentrations sometimes evoked a slow but significant increase in somatic $[Cl^-]_i$ (data not shown), which may be explained by GABA diffusing to the IPL and activating receptors on the axon terminals, where Cl^- influx then leads to Cl^- accumulation in the cell.

We next examined GABA responses at higher time resolution (Figures 7D–7G). These experiments were performed at 36°C, rather than at room temperature (RT) as the preceding experiments. This allowed us to optimize the time resolution of our measurements, because Cl^- binding to Clomeleon is accelerated at higher temperatures (W.S. and T.K., unpublished data). Again,

there was considerable variability in the GABA response of different types of bipolars.

In type 7 cells, GABA typically either elevated or had no effect upon $[Cl^-]_i$. Out of the eight identified type 7 cells, two responded to GABA with a small $[Cl^-]_i$ increase, while none showed a substantial $[Cl^-]_i$ decrease in their dendrites. In the first example for a type 7 cell (Figure 7D, left), $[Cl^-]_i$ was low, and no significant somatodendritic gradient was present. Application of GABA evoked a delayed $[Cl^-]_i$ increase in both compartments. In the second example (Figure 7D, right), the cell displays a small $[Cl^-]_i$ gradient, but GABA again evokes mainly a small delayed increase in $[Cl^-]_i$.

In type 9 cells, GABA caused $[Cl^-]_i$ to increase, decrease, or remain constant, depending upon the location of the response and the resting $[Cl^-]_i$ of the compartment. Of the 23 identified type 9 cells, seven responded to GABA with a transient $[Cl^-]_i$ decrease, which was followed by a delayed $[Cl^-]_i$ increase in five of the seven cells. In type 9 cells with relatively low $[Cl^-]_i$, GABA application resulted in a long-lasting increase in $[Cl^-]_i$ in both dendrites and somata (Figure 7E, left). In the example shown in this figure, the increase in dendritic $[Cl^-]_i$ was preceded by a small and transient decrease in $[Cl^-]_i$. In cases where the resting $[Cl^-]_i$ was high, GABA elicited a transient Cl^- efflux from dendritic varicosities (Figure 7E, right). This cell first showed a slight decrease in somatic $[Cl^-]_i$, possibly reflecting the dendritic response, which was followed by a small increase in somatic $[Cl^-]_i$. This secondary increase may be due to delayed diffusion of Cl^- from the axon terminals, and the delayed time course is consistent with the previous measurements of the time course of intracellular Cl^- diffusion (Kuner and Augustine, 2000).

To determine whether these GABA-evoked $[Cl^-]_i$ changes were mediated by GABA receptors, we examined the effects of GABA receptor antagonists. We simultaneously applied the $GABA_AR$-selective blocker GABAzine and the $GABA_CR$-selective blocker TPMPA, in addition to GABA (Figure 7F). These blockers completely abolished GABA-evoked $[Cl^-]_i$ changes in six out of six cells (one type 7 cell and five type 9 cells). Thus, the GABA-induced changes in $[Cl^-]_i$ were caused by activation of ionotropic GABA receptors.

To determine the influence of resting $[Cl^-]_i$ on the two components of the GABA response, the "initial" and "delayed" changes in $[Cl^-]_i$ were plotted as a function of resting $[Cl^-]_i$ for nine cells. The amplitude of the "initial" response was well correlated with resting $[Cl^-]_i$ (Pearson's $\rho = -0.82$). These data could be fit with a straight line that predicted a reversal of the direction of Cl^- flux at $[Cl^-]_i = 30$ mM. This $[Cl^-]_i$ corresponds to an E_{Cl} of -38 mV, which is close to the typical E_R of -42 mV for ON bipolar cells and suggests that E_R may be relatively homogenous among these cells. In contrast, "delayed" responses showed no significant dependence upon resting $[Cl^-]_i$ ($\rho = -0.36$).

In conclusion, the GABA response of type 7 and type 9 bipolar cells could be predicted from the steady-state $[Cl^-]_i$ of each cell type. Thus, the higher $[Cl^-]_i$ found in type 9 cell dendrites could indeed shift E_{Cl} to values sufficiently positive to E_R so that local Cl^- efflux occurred. In type 7 cell dendrites, a lower resting $[Cl^-]_i$ tended to produce influx of Cl^-.

Discussion

It has long been proposed that ON bipolar cells exhibit an axodendritic $[Cl^-]_i$ gradient—with high dendritic $[Cl^-]_i$—that inverses the polarity of the GABAergic feed-forward input from horizontal cells (Miller and Dacheux, 1983; Vardi and Sterling, 1994; Vardi et al., 2000). In the present study, we addressed this question by using ratiometric 2p microscopy to map $[Cl^-]_i$ in ON bipolars of a mouse line expressing Clomeleon, a genetically encoded fluorescent Cl^- indicator (Kuner and Augustine, 2000).

An Axodendritic $[Cl^-]_i$ Gradient in ON Bipolar Cells

We determined $[Cl^-]_i$ in three different compartments of type 7 and 9 ON cone bipolar cells (Figures 4A–4D). We found that the dendritic $[Cl^-]_i$ is significantly higher than the somatic $[Cl^-]_i$ (Figure 4E), whereas the axonal $[Cl^-]_i$, determined in cross-sections above the IPL, showed a trend toward lower $[Cl^-]_i$. These results are consistent with the bipolar cells exhibiting a $[Cl^-]_i$ gradient that extends from the distal dendrites to their axon terminals. Because Clomeleon is also sensitive to H^+, it is possible that gradients in intracellular pH could confound our measurements. We think this is unlikely for two reasons. First, the gradients reported by Clomeleon would require the dendrites to be 0.4 to 0.45 pH units more acidic than the rest of the bipolar cell, which seems unlikely under steady-state conditions (Amos and Richards, 1996). Second, our measurements indicate that the direction of GABA-evoked Cl^- fluxes in dendrites was predicted by the measured resting $[Cl^-]_i$, strongly indicating genuine $[Cl^-]_i$ gradients. Therefore, our results provide direct evidence for a pronounced axodendritic $[Cl^-]_i$ gradient in ON bipolar cells.

Our results complement and extend previous electrophysiological evidence for dendritic $[Cl^-]_i$ gradients. Gramicidin perforated-patch recordings have been used to estimate local E_{Cl} from the reversal potential of GABA-evoked currents (E_{GABA}). With this approach, Satoh and coworkers (Satoh et al., 2001) found that GABA application to the OPL depolarized rod bipolars but hyperpolarized both ON and OFF cone bipolars. They attributed this to E_{Cl} in rod bipolars being less negative than in cone bipolars; however, they did not report a significant $[Cl^-]_i$ gradient. In contrast, a recent study found axodendritic $[Cl^-]_i$ gradients of $\sim$21 mM in rod bipolars isolated from mouse retina (Varela et al., 2005). These gradients as well as the reported mean dendritic E_{Cl} (~ -33 mV) are very similar to our observations for type 9 cells. Billups and Attwell (2002) also used perforated-patch recordings and found small $[Cl^-]_i$ gradients of $\sim$4 mM in unidentified ON bipolars. Their gradients are nominally similar to our observations for type 7 cells, which may be underestimates, and are much smaller than the gradients that we observed in type 9 cells. It is likely that these discrepancies arise from methodological differences: perforated-patch recordings run the risk of perturbing the intracellular ionic composition, while Cl^- imaging is noninvasive and should not alter $[Cl^-]_i$ (Kuner and Augustine, 2000). Furthermore, interpretation of electrical recordings from bipolar cell somata relies critically on the site of GABA application, which, possibly with the exception of isolated cells, may be difficult to limit to a specific part of the neuron.

The earlier patch-clamp studies might also be influenced by pooling of different types of ON bipolars, which could have cell type-specific differences in dendritic $[Cl^-]_i$.

$[Cl^-]_i$ Gradient Consistent with Cl^- Transporter Expression

The existence of an axodendritic $[Cl^-]_i$ gradient was predicted from immunohistochemical data, in monkey and rabbit retina, showing the expression of the Cl^- importer NKCC1 on dendritic tips of both rod and ON cone bipolar cells, as well as on horizontal cells (Vardi et al., 2000). The Cl^- extruder KCC2 is found on dendrites and axon terminals of OFF bipolars, as well as on the axon terminals of rod bipolars, although its presence on axon terminals of ON cone bipolars is unclear (Vardi et al., 2000). A low axonal $[Cl^-]_i$ is required in bipolars, which receive major GABAergic and glycinergic inhibition from amacrine cells (e.g., Suzuki et al., 1990). Hence, both the reported distribution of Cl^- transporters and our results are consistent with the idea that Cl^- is accumulated in the dendrites and is extruded from axon terminals of ON bipolar cells. A direct connection between the two studies comes from our observation that inhibiting NKCCs and KCCs with Fu and Bm significantly reduced the gradient. Thus, these two Cl^- transporters are involved in establishing the $[Cl^-]_i$ gradient in bipolar cells. The fact that the inhibitors failed to abolish the $[Cl^-]_i$ gradient may simply indicate that other Cl^- transporters are involved as well (reviewed in Payne et al., 2003). This is reminiscent of the situation in the auditory brainstem, where a Cl^- importer different from NKCC1 is responsible for generating high $[Cl^-]_i$ during neuronal development (Balakrishnan et al., 2003).

Variability of Steady-State $[Cl^-]_i$

The $[Cl^-]_i$ in Clomeleon-positive bipolar cells was surprisingly variable, both within the same cell type as well as between different types of ON bipolars. This observation is consistent with large variations of E_{Cl} in bipolars reported by patch-clamp studies (Billups and Attwell, 2002; Satoh et al., 2001; Yamashita and Wässle, 1991). The mean somatic $[Cl^-]_i$ reported by the studies are similar to (22 mM; Billups and Attwell, 2002) or lower than (rod bipolars: 23 mM, ON cone bipolars: 13 mM; Satoh et al., 2001) our values (Figure 6). Considerable variations of $[Cl^-]_i$ even within a single cell type, such as the rod bipolar, have been described (Satoh et al., 2001; Varela et al., 2005). The $[Cl^-]_i$ ranges we found in type 7 and type 9 cells are consistent with this observation.

Developmental changes in $[Cl^-]_i$ (reviewed in Ben-Ari, 2002) are unlikely to account for the variability discussed here, because only adult mice ($\geq$2 months old) were used in our study. The variability in resting $[Cl^-]_i$ may involve changes in cellular volume, pH homeostasis (reviewed in Payne et al., 2003), and slow adaptations of $[Cl^-]_i$ in response to changes in resting membrane potential (Billups and Attwell, 2002).

Dendritic $[Cl^-]_i$ in Bipolar Cell Types

In the transgenic mouse line we studied, Clomeleon was expressed by four different morphological types of bipolar cells (Figure 1). Only three types of ON cone bipolars (Figure 2B), types 7, 8, and 9 (Ghosh et al., 2004), were visible in the in vitro retina. Since reliable $[Cl^-]_i$ measurements from the thin type 8 cell dendrites were not possible, for type-specific measurements we concentrated on type 7 and 9. The difference in somatodendritic $[Cl^-]_i$ gradient between type 7 and type 9 cells was remarkable: in type 9 the $[Cl^-]_i$ in the dendrites was on average 20 mM higher than in the soma, whereas in type 7 the dendritic $[Cl^-]_i$ was only 4 mM higher than in the soma (Figures 5D and 6B). This difference between bipolar types may be overestimated, because we were not able to restrict the measurements in type 7 solely to the distal dendritic tips, where $[Cl^-]_i$ should be highest. However, somatic $[Cl^-]_i$ was slightly lower in type 7 than in type 9, which would be consistent with a genuine difference in $[Cl^-]_i$ gradient between these cells. In light of these uncertainties, and the additional fact that we could examine only two identifiable cell types, it remains unclear whether significant $[Cl^-]_i$ gradients occur in the entire population of ON bipolars or are restricted to a few bipolar types, such as type 9.

GABA-Induced $[Cl^-]_i$ Responses

Bipolar cells express two subclasses of ionotropic GABA receptors (GABARs), $GABA_A$Rs and $GABA_C$Rs (reviewed in Wässle et al., 1998). The highest density of GABAR is found on their axon terminals, although GABARs are also found on bipolar cell dendrites (Enz et al., 1996; Greferath et al., 1994; Vardi and Sterling, 1994). We examined the function of the dendritic GABARs by applying GABA while monitoring $[Cl^-]_i$ in the dendrites and somata of Clomeleon-expressing bipolars (Figure 7). GABA-evoked $[Cl^-]_i$ changes were observed in 27% of these cells, and these responses were blocked by $GABA_{A/C}$R antagonists, indicating that the responses were mediated by ionotropic GABARs. The direction of the GABA-induced Cl^- flux in dendrite or soma could be predicted from the value of resting $[Cl^-]_i$ (Figure 7). In type 7 cells, GABA evoked a Cl^- influx (Figure 7D), consistent with their low mean $[Cl^-]_i$ and their small somatodendritic $[Cl^-]_i$ gradient. In contrast, GABA often evoked a transient Cl^- efflux in type 9 cells, which was followed by a delayed, overshooting Cl^- influx (Figure 7E). The Cl^- efflux from the dendrites is consistent with the high somatodendritic gradient we found in type 9 cells, while the delayed influx may be due to Cl^- diffusing from other parts of the cell, such as the axon terminals.

We have demonstrated that GABA generates Cl^- efflux in dendrites of type 9 bipolars, consistent with a depolarizing action required for an antagonistic receptive field organization (Figure 1). But surprisingly few of the 119 examined cells displayed detectable $[Cl^-]_i$ changes in response to GABA. In many of these cells, the predicted E_{Cl} was close to the typical E_R in ON bipolar cells, and therefore only a small GABA-evoked Cl^- flux would be expected. However, other cells did not respond even though their E_{Cl} was not close to the mean E_R of bipolar cells. It is possible that the E_R of these cells was closer than expected to E_{Cl} or that their dendrites had been mechanically damaged by the slicing procedure. It is more likely, though, that such cells generated responses that went undetected because the net flow of Cl^- was too small and/or too rapid to be detected by Clomeleon. The expected magnitude of GABA-induced $[Cl^-]_i$ changes can be estimated from typical GABA-elicited currents

measured electrophysiologically (e.g., Euler and Wässle, 1998). An average current flow of 10 pA for 2 s should change the $[Cl^-]_i$ in a small volume (e.g., a dendrite 20 μm long, 1 μm in diameter) by ~10 mM. This estimated change would be reduced by Cl^- transport, by Cl^- diffusion, and by the fact that GABA-evoked currents are partially carried by HCO_3^- (Bormann et al., 1987; Kaila et al., 1993). Nonetheless, this value is in line with the 2 to 12 mM changes in $[Cl^-]_i$ that were observed during GABA application (Figure 7F). On the other hand, it suggests that smaller—but still functionally relevant—GABA responses may not be detected by Clomeleon. The relatively slow kinetics of Cl^- binding to Clomeleon, which is in the range of 100–600 ms depending on pH, temperature, and $[Cl^-]_i$ (W.S. and T.K., unpublished data), may impede detection of fast transient changes in $[Cl^-]_i$.

GABA receptors are permeable not only to Cl^-, but also to HCO_3^- [with $p(HCO_3^-)/p(Cl^-) \sim 0.25$] (Bormann et al., 1987; Kaila et al., 1993). At physiological pH, the HCO_3^- reversal potential is close to 0 mV, and thus, $E_{GABA} > E_{Cl}$ (Dallwig et al., 1999). Hence, HCO_3^- fluxes usually mediate depolarization, suggesting that the initial $[Cl^-]_i$ decrease that we observed in type 9 cell dendrites represents an underestimate of the depolarizing effect of GABA on E_R. Furthermore, even when $E_{Cl} \sim E_R$ and no change in $[Cl^-]_i$ would result, GABAR-mediated HCO_3^- fluxes could still depolarize E_R (Dallwig et al., 1999). This in turn, will trigger hyperpolarizing Cl^- influx, until E_{Cl} reaches the new E_R. Such an effect may contribute to the delayed Cl^- influx we observed in many cells.

In principle, HCO_3^- efflux can decrease intracellular pH (pH_i), which in turn would increase the Cl^- sensitivity of Clomeleon (Kuner and Augustine, 2000). Such a pH_i shift theoretically could mimic a response like the delayed Cl^- influx. However, activity-dependent changes in pH_i, like those reported in hippocampal neurons (Luckermann et al., 1997; Pasternack et al., 1993), occur on a much slower timescale than the responses reported here and are consistent with compensatory production of new HCO_3^-, rather than with instantaneous HCO_3^- efflux (Ballanyi and Kaila, 1998). In fact, GABA application reportedly does not change pH_i in cultured rat cortical or hippocampal neurons (Dallwig et al., 1999; Kuner and Augustine, 2000). More importantly, the initial GABA-evoked decrease in $[Cl^-]_i$ (Figures 7E and 7F), which is likely to be most critical for circuit function, cannot be explained by a decrease in pH, which would mimic an *increase* in $[Cl^-]_i$. In conclusion, it is likely that Clomeleon is reporting GABA-evoked changes in $[Cl^-]_i$ rather than intracellular pH.

Function of $[Cl^-]_i$ Gradients in Bipolar Cells

Horizontal cells signal the background intensity and can affect bipolar cell responses both indirectly by modulating the photoreceptor output (feedback) or directly via GABAergic input to the bipolar cell dendrites (feed-forward). Photoreceptors have inhibitory surrounds created by horizontal cell feedback, via GABA (Baylor et al., 1971; Schwartz, 2002), ephaptic interactions (Kamermans and Fahrenfort, 2004), or modulation of extracellular pH (Barnes et al., 1993). Via the indirect feedback pathway, bipolars "inherit" the surround from the photoreceptors. This works for both ON and OFF bipolars, because the surround input is already "applied," before the photoreceptor signal is inverted at the synapse to the ON bipolar cell (Nomura et al., 1994). The direct feed-forward pathway should involve GABA release from horizontal cells, which is still somewhat enigmatic, because mammalian horizontal cells display some, but not all features of GABAergic neurons (reviewed in Grünert and Wässle, 1990; Haverkamp et al., 2000; Schwartz, 2002; Vardi and Sterling, 1994). Other possible GABA sources in the OPL are GABAergic interplexiform cells; however, at least in mouse retina they lack output synapses in the OPL (Gustincich et al., 1997). In the case of GABAergic feed-forward, ON and OFF bipolars require horizontal cell inputs of opposite polarity: GABAergic input to ON bipolar dendrites needs to be depolarizing to provide them with a corrective horizontal cell input analogous to that received by OFF bipolars. Our finding that type 9 bipolars possess high dendritic $[Cl^-]_i$ is consistent with this possibility.

The finding that type 7 ON bipolar cells appear to display only small $[Cl^-]_i$ gradients does not fit well with the view of high dendritic $[Cl^-]_i$ providing a general mechanism for antagonistic surrounds in ON bipolars. As discussed above, it is likely that these gradients were underestimated, so that type 7 cells may have gradients similar to those measured in type 9 cells. Nonetheless, we cannot exclude that the large $[Cl^-]_i$ gradients of type 9 cells fulfill some specialized function unique to these cells. It has been recently shown that type 9 cells selectively contact short wavelength-selective cones (S cones) (Haverkamp et al., 2005) and are therefore the mouse equivalent of the blue cone bipolars (Mariani, 1984), which participate in color processing (reviewed in Dacey and Packer, 2003). The only type of horizontal cell that exists in mouse (Peichl and González-Soriano, 1994) presumably contacts both cone types present—the S cones and the long wavelength-sensitive (L) cones—and therefore carries a different chromatic signal (S + L) than the blue cone bipolars (Haverkamp et al., 2005). Hence, antagonistic GABAergic input from HCs may in fact create a color-opponent signal in type 9 bipolars. Such color-opponent bipolar cells have been described in nonmammalian species (Kaneko, 1973) but have not yet been found in mammals.

In conclusion, we have demonstrated $[Cl^-]_i$ gradients that are formed in a relatively compact cell and apparently are used to differentially process signals relayed by the same transmitter at two subclasses of postsynaptic neurons, as previously postulated (Miller and Dacheux, 1983; Vardi and Sterling, 1994; Vardi et al., 2000). Intracellular $[Cl^-]_i$ gradients have been proposed to play functional roles in other parts of the brain (Hara et al., 1992; Kaneko et al., 2004; Kleene, 1993; Kuner and Augustine, 2000), suggesting that such $[Cl^-]_i$ gradients could be a general mechanism for neuronal information processing.

Experimental Procedures

Animals and Tissue Preparation

Transgenic mice expressing Clomeleon (CLM), a genetically encoded ratiometric fluorescent Cl^- indicator, under the *Thy1* promoter were used (Berglund et al., 2004; Feng et al., 2000; Kuner and Augustine, 2000). The animals (>2 months old) were killed by

an overdose of pentobarbital (Merial, Germany) applied intraperitoneally. All procedures were approved by the local animal care committee and were in accordance with the law of animal experimentation issued by the German Government (Tierschutzgesetz). The dissection was carried out in normal room light. The eyes were enucleated and transferred to a petri dish filled with oxygenized (95% O_2, 5% CO_2) Ames medium (Sigma-Aldrich, Germany) at RT. Each eye was cut open, and lens and vitreous were removed, leaving the posterior eyecup containing the retina.

Physiology

The retina was dissected from the eyecup. For whole-mount imaging, a piece of retina was placed (ganglion cells up) onto a cover slip coated with a cell adhesive (Cell-TAK, BD Biosciences, San Jose, CA). The cover slip was then placed in the recording chamber. In other experiments, retinal slices were used (Protti and Llano, 1998). In brief, a piece of retina (2–4 mm^2) was embedded in 2% agar dissolved in Ames medium (kept at 37°C). Then the agar was cooled and cut into a cube, which was transferred to a vibratome (Slicer HR2, Sigmann-Elektronik, Germany) for slicing (~200 μm thick). During the recordings, the retina was superfused with oxygenized Ames medium.

Anatomy

The posterior eye cup containing the retina was immediately immersed in 4% (w/v) paraformaldehyde (PFA) in 0.1 M phosphate buffer (pH 7.4) for 15–30 min. After fixation, the retina was dissected from the eyecup. The details for cutting sections and preparing the whole mounts have been described (Haverkamp et al., 2005).

Dye Injections

To reveal their complete axonal morphology, Clomeleon-positive bipolar cells in slices (living or fixed for 10–15 min with 4% PFA) were filled with dye using sharp electrodes. The electrodes were pulled on a P2000 laser puller (Sutter Instruments, Novato, CA) from borosilicate glass (O.D.: 1.0 mm, I.D.: 0.58 mm, with filament; Clark, Harvard Apparatus, Holliston, MA) and filled with 6 mM sulforhodamine 101 (Sigma-Aldrich) or 10 mM Alexa 594 (Molecular Probes, Eugene, OR) diluted in 0.2 M K-acetate.

Immunocytochemistry

For anatomy, staining with GFP antibody yields stronger fluorescence than Clomeleon alone (rabbit anti-GFP, 1:2000, Molecular Probes; mouse anti-GFP, 1:500, Chemicon, Temecula, CA). Cone pedicles were labeled by antibodies against GluR5, which is expressed at the postsynaptic sites (goat anti-GluR5N; 1:100; Santa Cruz) (Haverkamp et al., 2005). Antibodies were diluted in PBS (pH 7.4) containing 3% normal donkey serum, 0.5% Triton X-100, and 0.05% sodium azide. Immunocytochemical labeling was performed using the indirect fluorescence method. Cryostat and vibratome sections were incubated overnight in primary antibodies, followed by incubation (1 hr) in secondary antibodies conjugated either to Alexa TM 488 (Molecular Probes) or Cy3 (Dianova, Hamburg, Germany). Whole mounts were incubated for 2 days in the primary and for 2 hr in the secondary antibodies.

Confocal micrographs were taken using a Zeiss LSM Pascal fluorescence microscope (Oberkochen, Germany) equipped with a Plan-apochromate ×63/1.4 objective (2048 × 2048 pixels). Stacks of 12 sections were taken from the inner nuclear layer (INL) to the OPL (0.6 μm z axis steps) and collapsed into a single plane to reconstruct dendritic trees.

2p Microscopy

An upright 2p microscope (custom in-house design) equipped with a 20× water immersion lens (0.95 W, XLUMPlanFI, Olympus, Germany) was used for ratiometric Cl^- imaging. The excitation source was a mode-locked Ti/Sapphire laser (Mira-900; Coherent, Santa Clara, CA) tuned to 870 nm. The imaging software (CfNT; R. Stepnoski, Bell Labs; M. Müller, MPImF) allows simultaneous recordings of two fluorescent signals (CFP filter: 500 SP; YFP filter: 535 BP 50). Time series of images or z stacks were acquired from Clomeleon-expressing cells in whole mounts and slices. Various image geometries (64 × 8 to 256 × 256 pixels) with a scan rate of 2 ms/line (=62.5 to 2 frames/s) were used. The data were analyzed offline with IgorPro 5.0 (Wavemetrics, Lake Oswego, OR) and ImageJ (http://rsb.info.nih.gov/ij/).

Ratiometric Cl^- Imaging with Clomeleon Using 2p Excitation

Clomeleon consists of the Cl^--insensitive CFP linked by a short peptide to the Cl^--sensing YFP (Kuner and Augustine, 2000). This design allows ratiometric determination of $[Cl^-]_i$. With 2p microscopy, both CFP and YFP are excited directly, because the 2p cross spectra of the fluorophores overlap in the applicable range of excitation wavelengths (800–930 nm) (Elangovan et al., 2003). In this situation, YFP can fluoresce both by direct 2p excitation or by FRET via CFP. The ratio between the two excitation pathways depends on excitation wavelength, and average distance between the GFPs and is assumed to be constant.

The fluorescence of YFP is known to be pH dependent (Patterson et al., 1997; Wachter et al., 1997). As a consequence, the sensitivity of Clomeleon to Cl^- rises with increased $[H^+]$ (Kuner and Augustine, 2000). Intracellular pH of bipolar cells was determined using BCECF according to Haugh-Scheidt and Ripps (1998). Briefly, retinal slices were incubated for 30 min (at RT) in Ringer's solution (Biometra, Biomedizinische Analytik, Germany) containing 3 μM BCECF-AM-ester (Molecular Probes) and rinsed with Ringer's solution prior to imaging with a confocal microscope (Leica SP2, Wetzlar, Germany). The fluorescence ratio for 488 and 458 nm excitation ($R_{488/458}$) was measured at the soma (emission filter: 535 BP 50). For pH calibration, the cells were permeabilized using 10 μM Nigericin (Molecular Probes), and $R_{488/458}$ was determined at five different pH values (between 5.05 and 8.7) defined by the superfused medium. The data were well described by (Haugh-Scheidt and Ripps, 1998):

$$pH = pK_a - \log\left(\frac{R_{MAX} - R}{R - R_{MIN}} \cdot \frac{F_{base,458}}{F_{acid,458}}\right) \quad (1)$$

yielding a pK_A of 7.20 ± 0.07 (SD; n = 32 cells; data not shown). Intracellular pH in bipolars was 7.28 ± 0.14 (SD; n = 8 cells) and very close to pH 7.25 used for intracellular solutions in Cl^- calibration experiments. Nevertheless, this difference in pH results is a slight underestimation of $[Cl^-]_i$ (e.g., 10, 50 mM correspond to corrected values of 10.6, 52.9 mM, respectively; compare Figure 2E in Kuner and Augustine, 2000). Since pH is tightly regulated in neurons (Amos and Richards, 1996) at rest or under conditions of normal synaptic activity, errors induced by changes of intracellular pH are unlikely to bias our results.

Calibration of $[Cl^-]$ Measurements

The imaging system was calibrated as described (Kuner and Augustine, 2000). Briefly, cultured hippocampal neurons were infected with Sindbis virus particles encoding Clomeleon (Wimmer et al., 2004). Approximately 24 hr after transfection the cells were washed, transferred to the recording chamber of the 2p microscope, and perfused with oxygenized (95% O_2, 5% CO_2) Ringer's solution (Biometra). Patch electrodes (5–10 MΩ) were pulled from borosilicate glass (O.D.: 1.0 mm, I.D.: 0.58 mm, with filament; Hilgenberg, Germany) on a P-2000 laser puller (Sutter) and backfilled with intracellular solution containing the following: 10–125 mM KCl, 10–125 mM K-gluconate, 5 mM NMG-HEDTA, 20 mM HEPES (pH 7.25). A patch-clamp amplifier (Multiclamp) and the pClamp 8 software (both Axon Instruments, Union City, CA) were used for recordings. Before and after breaking into a cell, CFP and YFP signals were simultaneously acquired (Figure 3A). A ROI was placed over the cell body, and the fluorescence intensities were measured in both channels. After background subtraction in each channel (B_{YFP}, B_{CFP}) the YFP/CFP intensity ratio (R) was calculated:

$$R = \frac{F_{YFP} - B_{YFP}}{F_{CFP} - B_{CFP}} \quad (2)$$

We determined such YFP/CFP ratios for defined $[Cl^-]_i$ between 10 and 125 mM. The data points obtained with different $[Cl^-]$ in the pipette were well described by the ratiometric function (Figure 3C)

$$R = \frac{K'_D \cdot R_{MAX} + [Cl^-] \cdot R_{MIN}}{[Cl^-] + K'_D} \quad (3)$$

with maximal ratio (R_{MAX}), minimal ratio (R_{MIN}), and apparent dissociation constant (K'_D). While R_{MAX} and K'_D were free parameters, R_{MIN} was determined by quenching YFP fluorescence with 125 mM F^- (Kuner and Augustine, 2000). Using the data from 24 cells, we determined an R_{MIN} of 0.38, an R_{MAX} of 1.61 ± 0.02, and a K'_D

of 113 ± 6 mM. A second set of calibrations, necessitated after replacing the imaging electronics, yielded similar results (n = 11 cells; R_{MIN} = 0.33; R_{MAX} = 1.51 ± 0.02; K'_D = 107 ± 5 mM). Ratios were converted into $[Cl^-]_i$ using

$$[Cl^-] = K'_D \cdot \frac{R_{MAX} - R}{R - R_{MIN}} \quad (4)$$

Color coded maps of $[Cl^-]_i$ (1–100 mM) were generated from two-channel fluorescence images by averaging 15–20 frames (Figures 4, 5, and 7). $[Cl^-]_i$ > 100 mM is shown in white, $[Cl^-]_i$ < 1 mM and below threshold pixels (F < 10 units after background subtraction) is shown in black. Maps were spatially filtered (mean; 3 × 3 to 9 × 9 pixels depending on resolution).

Measurements of Steady-State $[Cl^-]_i$ and GABA-Evoked $[Cl^-]_i$ Changes

All $[Cl^-]_i$ are given as mean ± SEM. The significance of differences in $[Cl^-]_i$ was evaluated using one-way ANOVA and the Newman-Keul's post hoc test (significance at $p < 0.001$). Experiments were carried out at ~22ºC (RT) unless stated otherwise. Pharmacological agents were purchased from Sigma-Aldrich. Steady-state measurements of $[Cl^-]_i$ were performed in whole-mounted retina. Time series (15–20 frames) of bipolar cell dendrites, somata, and axon profiles were acquired (see Figure 4A). ROIs were drawn around the imaged compartments and pixels within were spatially averaged. For each frame, the YFP/CFP ratio was calculated (Equation 2), which then was converted into $[Cl^-]_i$ (Equation 4) and averaged over time.

To block the activity of the Cl^- transporters NKCC and KCC, we coapplied 25 μM Fu (4-Chloro-*N*-furfuryl-5-sulfamoylanthranilic acid) and 25 μM Bm [3-(Aminosulfonyl)-5-(butylamino)-4-phenoxybenzoic acid] with the medium supplemented with picrotoxin (50 μM; GABA antagonist) and strychnine (1 μM; glycine antagonist).

Effects of GABA on $[Cl^-]_i$ were studied in slices, where GABA (50–250 μM) was pressure applied via a pipette (tip diameter ~3 μm) directed to the outer half of the retina ~20–30 μm above the slice surface. To test if GABA responses were mediated by GABA receptors, we coapplied antagonists via a double-barreled pipette with 150 μM GABA in one barrel and GABA, GABAzine (SR-95531; 50 μM; $GABA_A$-selective), and TPMPA (1,2,5,6-tetrahydro-pyridine-4-yl-methylphosphinic acid; 50 μM; $GABA_C$-selective) in the second barrel. In four cells (3% of all cells), we observed GABA-evoked fluorescence changes, which translated into unrealistic changes in somatic $[Cl^-]_i$ of up to 100 mM. These cells were excluded from the analysis.

With prolonged measurements bleaching can pose a problem, because YFP bleaches more rapidly than CFP. The result is a slow but steady apparent increase in $[Cl^-]_i$. We did not compensate for bleaching but discarded cells where bleaching occurred. To be able to measure $[Cl^-]_i$ in more than one focal plane, e.g., to capture dendrites in sliced retina, we took image stacks at different time points before, during, and after GABA application. For analysis, the stacks were collapsed. We also performed time-lapsed recordings of GABA responses (recorded at 7.8–31.25 Hz; boxcar-filtered; 960–1960 ms window).

Acknowledgments

We thank A. Migalla and T. Schweizer for excellent technical assistance, H. Wässle for helpful discussions, and U. Misgeld for critical comments on earlier versions of the manuscript. The Cl^- imaging experiments were performed in W. Denk's laboratory. This study was supported by the Max-Planck Society and by NIH grant MH073166, awarded to G.J.A. and G.F.

Received: April 7, 2005
Revised: September 1, 2005
Accepted: October 31, 2005
Published: January 4, 2006

References

Akaike, N. (1994). Glycine responses in rat CNS neurons studied with gramicidin perforated patch recording. Jpn. J. Physiol. *44*, S113–S118.

Amos, B.J., and Richards, C.D. (1996). Intrinsic hydrogen ion buffering in rat CNS neurones maintained in culture. Exp. Physiol. *81*, 261–271.

Balakrishnan, V., Becker, M., Löhrke, S., Nothwang, H.G., Guresir, E., and Friauf, E. (2003). Expression and function of chloride transporters during development of inhibitory neurotransmission in the auditory brainstem. J. Neurosci. *23*, 4134–4145.

Ballanyi, K., and Kaila, K. (1998). Activity-evoked changes in intracellular pH. In pH and Brain Function, K. Kaila and B.R. Ransom, eds. (New York: Wiley-Liss), pp. 291–308.

Barnes, S., Merchant, V., and Mahmud, F. (1993). Modulation of transmission gain by protons at the photoreceptor output synapse. Proc. Natl. Acad. Sci. USA *90*, 10081–10085.

Baylor, D.A., Fuortes, M.G., and O'Bryan, P.M. (1971). Receptive fields of cones in the retina of the turtle. J. Physiol. *214*, 265–294.

Ben-Ari, Y. (2002). Excitatory actions of GABA during development: the nature of the nurture. Nat. Rev. Neurosci. *3*, 728–739.

Berglund, K., Dunbar, R.L., Lee, P., Feng, G., and Augustine, G.J. (2004). Imaging synaptic inhibition with Clomeleon, a genetically encoded chloride indicator. In Imaging in Neuroscience and Development: A Laboratory Manual, R. Yuste and A. Konnerth, eds. (New York: Cold Spring Harbor Laboratory Press).

Billups, D., and Attwell, D. (2002). Control of intracellular chloride concentration and GABA response polarity in rat retinal ON bipolar cells. J. Physiol. *545*, 183–198.

Bormann, J., Hamill, O.P., and Sakmann, B. (1987). Mechanism of anion permeation through channels gated by glycine and gamma-aminobutyric acid in mouse cultured spinal neurons. J. Physiol. *385*, 243–286.

Dacey, D.M., and Packer, O.S. (2003). Colour coding in the primate retina: diverse cell types and cone-specific circuitry. Curr. Opin. Neurobiol. *13*, 421–427.

Dacey, D., Packer, O.S., Diller, L., Brainard, D., Peterson, B., and Lee, B. (2000). Center surround receptive field structure of cone bipolar cells in primate retina. Vision Res *40*, 1801–1811.

Dallwig, R., Deitmer, J.W., and Backus, K.H. (1999). On the mechanism of GABA-induced currents in cultured rat cortical neurons. Pflügers Arch. *437*, 289–297.

Elangovan, M., Wallrabe, H., Chen, Y., Day, R.N., Barroso, M., and Periasamy, A. (2003). Characterization of one- and two-photon excitation fluorescence resonance energy transfer microscopy. Methods *29*, 58–73.

Enz, R., Brandstätter, J.H., Wässle, H., and Bormann, J. (1996). Immunocytochemical localization of the GABAc receptor rho subunits in the mammalian retina. J. Neurosci. *16*, 4479–4490.

Euler, T., and Masland, R.H. (2000). Light-evoked responses of bipolar cells in a mammalian retina. J. Neurophysiol. *83*, 1817–1829.

Euler, T., and Wässle, H. (1998). Different contributions of GABAA and GABAC receptors to rod and cone bipolar cells in a rat retinal slice preparation. J. Neurophysiol. *79*, 1384–1395.

Feng, G., Mellor, R.H., Bernstein, M., Keller-Peck, C., Nguyen, Q.T., Wallace, M., Nerbonne, J.M., Lichtman, J.W., and Sanes, J.R. (2000). Imaging neuronal subsets in transgenic mice expressing multiple spectral variants of GFP. Neuron *28*, 41–51.

Ghosh, K.K., Bujan, S., Haverkamp, S., Feigenspan, A., and Wässle, H. (2004). Types of bipolar cells in the mouse retina. J. Comp. Neurol. *469*, 70–82.

Greferath, U., Grünert, U., Müller, F., and Wässle, H. (1994). Localization of $GABA_A$ receptors in the rabbit retina. Cell Tissue Res. *276*, 295–307.

Grünert, U., and Wässle, H. (1990). GABA-like immunoreactivity in the macaque monkey retina: a light and electron microscopic study. J. Comp. Neurol. *297*, 509–524.

Grynkiewicz, G., Poenie, M., and Tsien, R.Y. (1985). A new generation of Ca2+ indicators with greatly improved fluorescence properties. J. Biol. Chem. *260*, 3440–3450.

Gustincich, S., Feigenspan, A., Wu, D.K., Koopman, L.J., and Raviola, E. (1997). Control of dopamine release in the retina: A transgenic approach to neural networks. Neuron *18*, 723–736.

Hara, M., Inoue, M., Yasukura, T., Ohnishi, S., Mikami, Y., and Inagaki, C. (1992). Uneven distribution of intracellular Cl− in rat hippocampal neurons. Neurosci. Lett. *143*, 135–138.

Hare, W.A., and Owen, W.G. (1990). Spatial organization of the bipolar cell's receptive field in the retina of the tiger salamander. J. Physiol. *421*, 223–245.

Hare, W.A., and Owen, W.G. (1996). Receptive field of the retinal bipolar cell—a pharmacological study in the tiger salamander. J. Neurophysiol. *76*, 2005–2019.

Haugh-Scheidt, L., and Ripps, H. (1998). pH regulation in horizontal cells of the skate retina. Exp. Eye Res. *66*, 449–463.

Haverkamp, S., Grünert, U., and Wässle, H. (2000). The cone pedicle, a complex synapse in the retina. Neuron *27*, 85–95.

Haverkamp, S., Wässle, H., Duebel, J., Kuner, T., Augustine, G.J., Feng, G., and Euler, T. (2005). The primordial, blue-cone color system of the mouse retina. J. Neurosci. *25*, 5438–5445.

Kaila, K., Voipio, J., Paalasmaa, P., Pasternack, M., and Deisz, R.A. (1993). The role of bicarbonate in GABAA receptor-mediated IPSPs of rat neocortical neurones. J. Physiol. *464*, 273–289.

Kamermans, M., and Fahrenfort, I. (2004). Ephaptic interactions within a chemical synapse: hemichannel-mediated ephaptic inhibition in the retina. Curr. Opin. Neurobiol. *14*, 531–541.

Kaneko, A. (1970). Physiological and morphological identification of horizontal, bipolar and amacine cells in goldfish retina. J. Physiol. *207*, 623–633.

Kaneko, A. (1973). Receptive field organization of bipolar and amacrine cells in the goldfish retina. J. Physiol. *235*, 133–153.

Kaneko, H., Putzier, I., Frings, S., Kaupp, U.B., and Gensch, T. (2004). Chloride accumulation in mammalian olfactory sensory neurons. J. Neurosci. *24*, 7931–7938.

Kleene, S.J. (1993). Origin of the chloride current in olfactory transduction. Neuron *11*, 123–132.

Kuner, T., and Augustine, G.J. (2000). A genetically encoded ratiometric indicator for chloride: Capturing chloride transients in cultured hippocampal neurons. Neuron *27*, 447–459.

Luckermann, M., Trapp, S., and Ballanyi, K. (1997). GABA- and glycine-mediated fall of intracellular pH in rat medullary neurons in situ. J. Neurophysiol. *77*, 1844–1852.

Mariani, A.P. (1984). Bipolar cells in monkey retina selective for the cones likely to be blue-sensitive. Nature *308*, 184–186.

Miller, R.F., and Dacheux, R.F. (1976). Synaptic organization and ionic basis of on and off channels in mudpuppy retina. I. Intracellular analysis of chloride-sensitive electrogenic properties of receptors, horizontal cells, bipolar cells, and amacrine cells. J. Gen. Physiol. *67*, 639–659.

Miller, R.F., and Dacheux, R.F. (1983). Intracellular chloride in retinal neurons: measurement and meaning. Vision Res *23*, 399–411.

Nomura, A., Shigemoto, R., Nakamura, Y., Okamoto, N., Mizuno, N., and Nakanishi, S. (1994). Developmentally regulated postsynaptic localization of a metabotropic glutamate receptor in rat rod bipolar cells. Cell *77*, 361–369.

Pasternack, M., Voipio, J., and Kaila, K. (1993). Intracellular carbonic anhydrase activity and its role in GABA-induced acidosis in isolated rat hippocampal pyramidal neurons. Acta Physiol. Scand. *148*, 229–231.

Patterson, G.H., Knobel, S.M., Sharif, W.D., Kain, S.R., and Piston, D.W. (1997). Use of the green fluorescent protein and its mutants in quantitative fluorescence microscopy. Biophys. J. *73*, 2782–2790.

Payne, J.A., Rivera, C., Voipio, J., and Kaila, K. (2003). Cation-chloride co-transporters in neuronal communication, development and trauma. Trends Neurosci. *26*, 199–206.

Peichl, L., and González-Soriano, J. (1994). Morphological types of horizontal cell in rodent retinae: a comparison of rat, mouse, gerbil and guinea pig. Vis. Neurosci. *11*, 501–517.

Protti, D.A., and Llano, I. (1998). Calcium currents and calcium signaling in rod bipolar cells of rat retinal slices. J. Neurosci. *18*, 3715–3724.

Satoh, H., Kaneda, M., and Kaneko, A. (2001). Intracellular chloride concentration is higher in rod bipolar cells than in cone bipolar cells of the mouse retina. Neurosci. Lett. *310*, 161–164.

Schwartz, E.A. (2002). Transport-mediated synapses in the retina. Physiol. Rev. *82*, 875–891.

Stone, S., and Schutte, M. (1991). Physiological and morphological properties of off- and on-center bipolar cells in the Xenopus retina: effects of glycine and GABA. Vis. Neurosci. *7*, 363–376.

Suzuki, S., Tachibana, M., and Kaneko, A. (1990). Effects of glycine and GABA on isolated bipolar cells of the mouse retina. J. Physiol. *421*, 645–662.

Toyoda, J., and Kujiraoka, T. (1982). Analyses of bipolar cell responses elicited by polarization of horizontal cells. J. Gen. Physiol. *79*, 131–145.

Vardi, N., and Sterling, P. (1994). Subcellular localization of GABAA receptor on bipolar cells in macaque and human retina. Vision Res *34*, 1235–1246.

Vardi, N., Zhang, L.L., Payne, J.A., and Sterling, P. (2000). Evidence that different cation chloride cotransporters in retinal neurons allow opposite responses to GABA. J. Neurosci. *20*, 7657–7663.

Varela, C., Blanco, R., and De la Villa, P. (2005). Depolarizing effect of GABA in rod bipolar cells of the mouse retina. Vision Res. *45*, 2659–2667.

Wachter, R.M., King, B.A., Heim, R., Kallio, K., Tsien, R.Y., Boxer, S.G., and Remington, S.J. (1997). Crystal structure and photodynamic behavior of the blue emission variant Y66H/Y145F of green fluorescent protein. Biochemistry *36*, 9759–9765.

Wässle, H., Koulen, P., Brandstätter, J.H., Fletcher, E.L., and Becker, C.M. (1998). Glycine and GABA receptors in the mammalian retina. Vision Res *38*, 1411–1430.

Werblin, F.S. (1974). Control of retinal sensitivity. II. Lateral interactions at the outer plexiform layer. J. Gen. Physiol. *63*, 62–87.

Werblin, F.S., and Dowling, J.E. (1969). Organization of the retina of the mudpuppy, Necturus maculosus. II. Intracellular recording. J. Neurophysiol. *32*, 339–355.

Wimmer, V.C., Nevian, T., and Kuner, T. (2004). Targeted in vivo expression of proteins in the calyx of Held. Pflügers Arch. *449*, 319–333.

Yamashita, M., and Wässle, H. (1991). Reversal potential of GABA-induced currents in rod bipolar cells of the rat retina. Vis. Neurosci. *6*, 399–401.

Yang, X.L., and Wu, S.M. (1991). Feedforward lateral inhibition in retinal bipolar cells: input-output relation of the horizontal cell-depolarizing bipolar cell synapse. Proc. Natl. Acad. Sci. USA *88*, 3310–3313.